Collective Effects in Second-Harmonic Generation from Split-Ring-Resonator Arrays

S. Linden,[1,2] F. B. P. Niesler,[1] J. Förstner,[3] Y. Grynko,[3] T. Meier,[3] and M. Wegener[1]

[1]*Institute of Nanotechnology, Institute of Applied Physics, and DFG-Center for Functional Nanostructures (CFN), Karlsruhe Institute of Technology (KIT), 76128 Karlsruhe, Germany*

[2]*Physikalisches Institut, University of Bonn, 53115 Bonn, Germany*

[3]*Physics Department, University Paderborn, 33098 Paderborn, Germany*

(Received 7 February 2012; published 6 July 2012)

Optical experiments on second-harmonic generation from split-ring-resonator square arrays show a nonmonotonic dependence of the conversion efficiency on the lattice constant. This finding is interpreted in terms of a competition between dilution effects and linewidth or near-field changes due to interactions among the individual elements in the array.

DOI: 10.1103/PhysRevLett.109.015502 PACS numbers: 81.05.Xj

Tailored man-made effective materials called metamaterials are widely known for supporting unprecedented linear optical properties, largely based on creating artificial magnetism via magnetic split-ring resonators and variations thereof [1–6]. Nonlinear optical properties of metamaterials are at least of equal scientific and technological interest [7,8]; however, they have been studied experimentally to a much lesser extent [9–16]. Here, the long-term vision is to achieve optical switching or nonlinear frequency conversion with efficiencies that are orders of magnitude above those of natural substances. So far, however, experiments lag far behind this ambitious goal. This status is largely due to a lack of fundamental understanding of the underlying physics. For example, even the microscopic source of the constituent metals' (e.g., gold or silver) optical nonlinearity is still the subject of scientific controversy [17–19]. Nevertheless, the "hot spots" [20] known from rough metal films raise hopes that huge enhancements might eventually be reproducibly achievable in rationally designed and lithographically fabricated nonlinear-optical metamaterial structures. For example, very promising results have been obtained regarding high-harmonic generation from noble gases near bow-tie antennas [21].

One design strategy could be to create a tiny individual building block (meta-atom), exhibiting large local-field enhancement, add a nonlinear constituent to these hot spots, and then pack these meta-atoms as densely as possible to form an effective nonlinear metamaterial. In this Letter, we show experimentally and theoretically that collective effects of the meta-atoms can substantially alter this picture, leading to optimal behavior at some intermediate packing density of the meta-atoms. Second-harmonic generation from split-ring resonators with a fundamental resonance at around 1.4 μm wavelength serves as an example.

The samples for our experiments have been fabricated using standard electron-beam lithography and standard high-vacuum evaporation of gold, followed by a lift-off procedure. We use split-ring resonators (SRR) as the paradigmatic building block of metamaterials. The SRR are arranged on a square lattice with lattice constant a. To study the effect of packing, or equivalently to study the second-harmonic generation (SHG) efficiency versus a, a large set of samples has been fabricated in which we vary the electron-beam exposure dose for each of the different lattice constants ($a = 280$, 300, 325, 350, 400, 450, 500 nm). From this set we pick those arrays that exhibit a nearly constant resonance wavelength (about 1.4 μm) of the fundamental SRR resonance. This choice aims at easing the interpretation of the nonlinear-optical experiments. It becomes apparent from Fig. 1 that the resulting

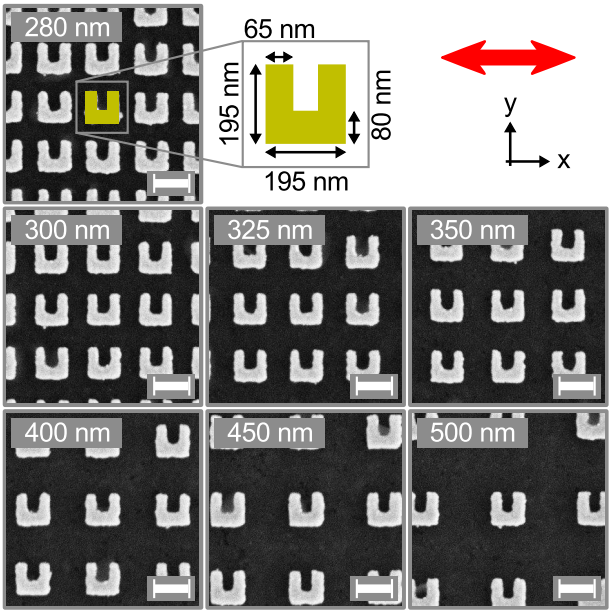

FIG. 1 (color online). Selected top-view electron micrographs of the gold split-ring-resonator (SRR) square arrays used in our experiments. The gold film thickness is 30 nm, the lattice constant a is indicated in each case, and the footprint of each array is 100×100 μm. The red arrow illustrates the incident linear polarization of light used throughout this Letter. The length of the white scale bars is 200 nm. The yellow SRR on the top illustrates the geometrical parameters used for the calculations in Fig. 3 for *all* a.

size variations of the SRR for the different arrays are extremely small. This aspect is important because resulting changes in the individual SRR properties (e.g., damping) would be an artifact (also see [5]). All SRR arrays have a footprint of 100×100 μm and a gold film thickness of 30 nm.

Fig. 2(a) exhibits the measured linear-optical extinction spectra (negative decadic logarithm of the intensity transmittance) for normal incidence of light, depicted on a false-color scale. As expected from the dilution and consistent with previous results, we find a monotonic decay of the peak extinction of the fundamental resonance versus lattice constant. The small wiggles in the resonance position are due to small SRR size variations among the different arrays. The same aspects hold true for a higher-order resonance centered around 750 nm wavelength. Panel (c) of Fig. 2 reveals the measured SHG signal versus center wavelength of the incident laser pulses that are derived from a tunable optical parametric amplifier (OPA) and versus lattice constant, again depicted on a false-color scale. To eliminate any parasitic effects due to changes in the pulse duration, pulse energy, pulse shape, beam divergence etc. when tuning the OPA, the SHG signals from the SRR arrays are consistently normalized to the off-resonant SHG from a quartz surface. Details of this setup have been published previously [12]. In sharp contrast to the linear optical data, the SHG signals show a nonmonotonic behavior versus lattice constant. The SHG signal in Fig. 2(c) at 1395 nm excitation wavelength first rises from normalized levels of 1.3 at 280 nm lattice constant to SHG levels of 3 at 400 nm lattice constant. For yet larger lattice constants, the SHG rolls off, reaching a level of 0.8 at 500 nm lattice constant. To rule out any effects from the slightly varying SRR resonance wavelength, we have taken complete SHG spectra for each lattice constant. At each lattice constant, we find the same general nonmonotonic behavior. The decay of the SHG signal at very large lattice constants is determined by the decreasing number of oscillators per area or per volume. After all, zero SRR density will surely lead to zero SHG from the SRR array. This dilution corresponds to a scaling of the second-order nonlinear polarization $\propto 1/a^2$; hence, the SHG signal intensity scales $\propto 1/a^4$. In the opposite limit of very small a, the SRR eventually touch (which happens at $a = 195$ nm, see Fig. 1), the SRR resonance disappears, and both the extinction and the SHG signal are expected to decrease. However, as becomes clear from the extinction spectra in Fig. 2(a), a well-defined SRR resonance is observed for all lattice constants investigated. Even at the smallest lattice constant of $a = 280$ nm, no drop of the extinction with decreasing a is found. The initial rise of the SHG signal versus lattice constant for small a must, thus, have a different origin.

Intuitively, one might be tempted to suspect some sort of diffractive effect, e.g., brought about by the Wood (or Rayleigh) anomaly. Fortunately, closely similar samples have recently been characterized in detail in linear-optical experiments [5] (also see [3]). For normal incidence of light at the fundamental resonance

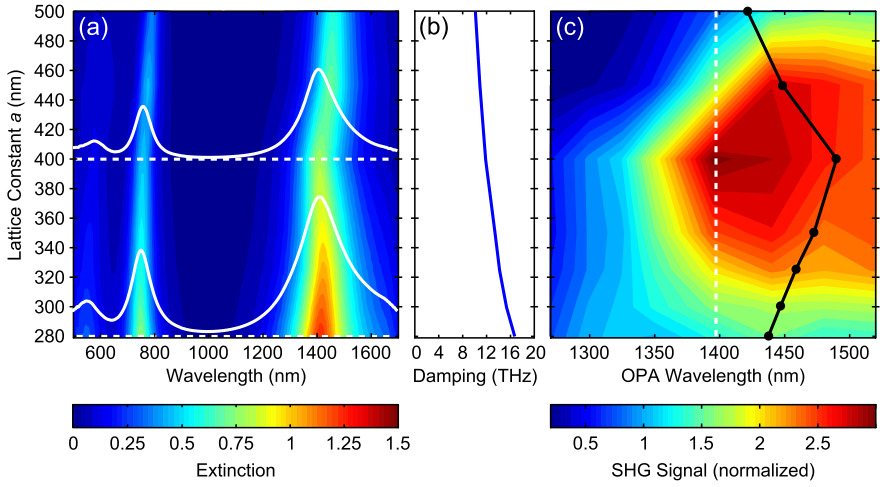

FIG. 2 (color online). (a) Normal-incidence, linear-optical extinction (negative decadic logarithm of the measured intensity transmittance) versus wavelength and versus lattice constant a of the SRR square arrays, plotted on a false-color scale. Two selected cuts through these data are shown by the white curves. The white dashed horizontal lines are the respective zero levels. (b) Damping versus lattice constant as obtained from Lorentzian fits to the data in (a). (c) Second-harmonic generation (SHG) signal from the same SRR arrays versus incident fundamental wavelength of the optical parametric amplifier (OPA) and versus a. The SHG signal is normalized to a quartz reference and plotted on a false-color scale. A selected cut through these data versus lattice constant a is shown by the black curve. The white dashed vertical line is the zero level. Note the nonmonotonic behavior of the SHG, whereas the linear properties in (a) show a monotonic decay with increasing a.

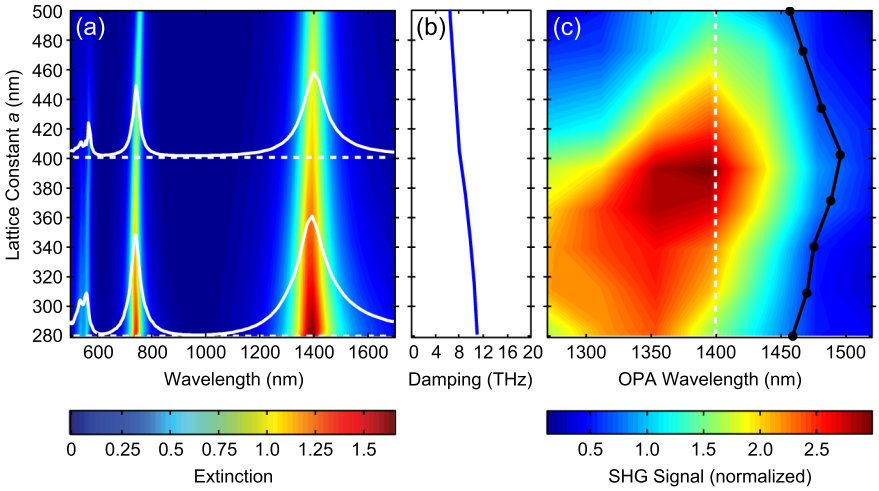

FIG. 3 (color online). Calculations corresponding to the experiment in Fig. 2. The representation is the same, allowing for direct comparison. The geometrical parameters used for the split-ring resonators are shown at the top of Fig. 1. Panel (c) uses the hydrodynamic Maxwell-Vlasov theory to describe the nonlinear response of the gold split-ring resonators.

wavelength, the Wood anomaly occurs at lattice constants larger than about 900 nm, i.e., diffraction of the incident light into the SRR plane can be ruled out under the present conditions. Diffraction of the SHG signal would lead to a decrease rather than to the observed initial increase in the (zeroth-order) forward direction but may well contribute to the expected decay of the SHG signal at larger lattice constants. Yet, these linear optical experiments [5] also revealed a pronounced decrease of the linewidth of the SRR resonance with increasing lattice constant. For the present samples, the damping γ as obtained from Lorentzian fits to the data shown in Fig. 2(a) decreases from $\gamma = 16$ THz at $a = 280$ nm nearly linearly to $\gamma = 10$ THz at $a = 500$ nm (see Fig. 2(b)). This dependence can be interpreted as being due to a retarded long-range interaction among the SRR in the array [5]. The linewidth of the resonance enters sensitively into the second-order nonlinear-optical susceptibility $\chi^{(2)}$—even in the simple textbook nonlinear oscillator model [22]. Smaller damping leads to larger resonant $\chi^{(2)}$ [22]. In addition, the amplitude of local-field-enhancement effects also increases with decreasing damping. The overall SHG intensity therefore further increases with decreasing damping. Moreover, the spatial distribution of the local SRR fields also enters sensitively into the SHG conversion efficiency. Combined with the trivial dilution effect discussed above, these three aspects can qualitatively explain the measured nonmonotonic behavior of the SHG signal versus lattice constant.

To test this qualitative reasoning quantitatively and to rule out any experimental artifacts, we have performed numerical calculations using the discontinuous Galerkin time-domain method [23,24] for the experimentally investigated gold split-ring-resonator square arrays. We describe the optical response of the metal by the

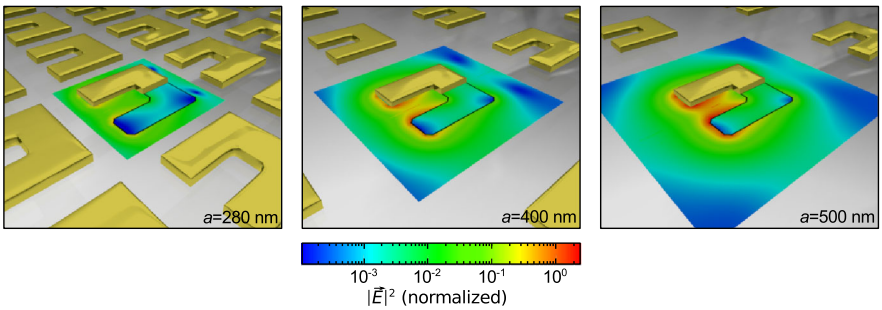

FIG. 4 (color online). Near-field distributions for three different lattice constants a as obtained from numerical calculations with parameters as in Fig. 3. The square modulus of the electric-field vector, $|\vec{E}|^2$, at the fundamental SRR resonance frequency is shown on a logarithmic false-color scale. The normalization is the same for all three panels. For clarity, half of the golden SRR in one unit cell is made transparent. For the lattice constants shown, an increase of the SRR lattice constant a leads to an increase of the strength of the near and internal fields and, hence, to a larger SHG far-field signal. At yet larger lattice constants, this trend is reversed by the trivial dilution effect.

state-of-the-art hydrodynamic Maxwell-Vlasov theory [25,26]. Its linear limit corresponds to the Drude free-electron model, for which we have chosen a plasma frequency $\omega_{\mathrm{pl}} = 1.33 \times 10^{16}$ rad/s, a collision frequency $\omega_{\mathrm{col}} = 8 \times 10^{13}$ rad/s, and a background dielectric constant of $\epsilon_\infty = 9.84$. The refractive index of the glass substrate is taken as $n = 1.46$. The geometric SRR parameters (which are the same for all lattice constants a) are according to the yellow SRR in Fig. 1. Fig. 3(a) shows calculated linear-optical extinction spectra. These calculations reproduce the experimentally observed monotonic decrease of the extinction peak and of the damping [see Fig. 3(b)] with increasing lattice constant a. The nonlinear SHG calculations are depicted in Fig. 3(c). We find a pronounced maximum of the SHG signal versus lattice constant at about $a = 400$ nm throughout the entire spectral resonance. This nonmonotonic behavior versus lattice constant nicely reproduces the experimental findings shown in Fig. 2(c). Thus, the numerical results strongly support the above qualitative reasoning in that the SHG signal is strongly influenced by collective effects via the SRR damping as well as via the SRR near-field distributions.

Since the detailed microscopic mechanism of the metal nonlinearity is still subject to debates (see above), we have also performed calculations using other models for the nonlinearity. In particular, this includes a simple generic treatment with an effective instantaneous second-order nonlinear susceptibility for the gold SRR. The results (shown in the Supplemental Material [27] together with details on the model) confirm the fundamental nature of the reported nonmonotonic behavior. However, none of these calculations is able to precisely reproduce the asymmetry of the spectral SRR resonance shown in Fig. 2(c).

Fig. 4 illustrates the origin of the collective effects as already qualitatively discussed above. Indeed, the SRR near fields within one unit cell at the fundamental resonance frequency depend on the lattice constant. Stronger near fields lead to stronger internal currents and hence to larger SHG signals. Once the SRR are separated by more than the extent of their near-fields, the near fields no longer increase with increasing a and the SHG signal eventually decreases due to the trivial dilution effect.

In conclusion, we have observed a nonmonotonic behavior of the resonant second-order nonlinear conversion efficiency in split-ring-resonator arrays versus packing density. The corresponding theoretical modeling indicates that this finding is a rather general phenomenon that is based on collective effects among the metamaterial building blocks and that should occur in many nonlinear metamaterials. Thus, future experiments aiming at achieving large effective (high-order) optical nonlinearities should keep these collective effects in mind. The same very likely holds true for experiments aimed at compensating metamaterial losses by parametric gain or by stimulated emission.

We acknowledge support by the DFG-Center for Functional Nanostructures (CFN) via subproject A1.5, the Deutsche Forschungsgemeinschaft (DFG) through the priority program SPP 1391, the research training group GRK 1464, and the Emmy-Noether program. The project METAMAT is supported by the Bundesministerium für Bildung und Forschung (BMBF). The Ph.D. education of F. B. P. Niesler is embedded in the Karlsruhe School of Optics & Photonics (KSOP). S. Linden and F. B. P. Niesler contributed equally to this work.

[1] S. Linden, C. Enkrich, M. Wegener, J. Zhou, T. Koschny, and C. M. Soukoulis, Science **306**, 1351 (2004).
[2] V. M. Shalaev, Nature Photon. **1**, 41 (2007).
[3] I. Sersic, M. Frimmer, E. Verhagen, and A. F. Koenderink, Phys. Rev. Lett. **103**, 213902 (2009).
[4] M. Decker, R. Zhao, C. M. Soukoulis, S. Linden, and M. Wegener, Opt. Lett. **35**, 1593 (2010).
[5] M. Decker, N. Feth, C. M. Soukoulis, S. Linden, and M. Wegener, Phys. Rev. B **84**, 085416 (2011).
[6] C. M. Soukoulis and M. Wegener, Nature Photon. **5**, 523 (2011).
[7] J. Pendry, A. Holden, D. Robbins, and W. Stewart, IEEE Trans. Microwave Theory Tech. **47**, 2075 (1999).
[8] A. A. Zharov, I. V. Shadrivov, and Y. S. Kivshar, Phys. Rev. Lett. **91**, 037401 (2003).
[9] M. W. Klein, C. Enkrich, M. Wegener, and S. Linden, Science **313**, 502 (2006).
[10] N. Feth, S. Linden, M. W. Klein, M. Decker, F. B. P. Niesler, Y. Zeng, W. Hoyer, J. Liu, S. W. Koch, J. V. Moloney *et al.*, Opt. Lett. **33**, 1975 (2008).
[11] F. B. P. Niesler, N. Feth, S. Linden, J. Niegemann, J. Gieseler, K. Busch, and M. Wegener, Opt. Lett. **34**, 1997 (2009).
[12] F. B. P. Niesler, N. Feth, S. Linden, and M. Wegener, Opt. Lett. **36**, 1533 (2011).
[13] E. Kim, F. Wang, W. Wu, Z. Yu, and Y. R. Shen, Phys. Rev. B **78**, 113102 (2008).
[14] S. Tang, D. J. Cho, H. Xu, W. Wu, Y. R. Shen, and L. Zhou, Opt. Express **19**, 18283 (2011).
[15] S. Kujala, B. K. Canfield, M. Kauranen, Y. Svirko, and J. Turunen, Phys. Rev. Lett. **98**, 167403 (2007).
[16] B. K. Canfield, H. Husu, J. Laukkanen, B. Bai, M. Kuittinen, J. Turunen, and M. Kauranen, Nano Lett. **7**, 1251 (2007).
[17] F. X. Wang, F. J. Rodriguez, W. M. Albers, R. Ahorinta, J. E. Sipe, and M. Kauranen, Phys. Rev. B **80**, 233402 (2009).
[18] Y. Zeng and J. Moloney, Opt. Lett. **34**, 2844 (2009).
[19] J. E. Sipe, V. C. Y. So, M. Fukui, and G. I. Stegeman, Phys. Rev. B **21**, 4389 (1980).
[20] M. I. Stockman, D. J. Bergman, C. Anceau, S. Brasselet, and J. Zyss, Phys. Rev. Lett. **92**, 057402 (2004).
[21] S. Kim, J. Jin, Y. J. Kim, I. Y. Park, Y. Kim, and S. W. Kim, Nature (London) **453**, 757 (2008).

[22] R. Boyd, *Nonlinear Optics* (Elsevier LTD, Oxford, 2000), 2nd ed.

[23] J. S. Hesthaven, *Nodal Discontinuous Galerkin Methods: Algorithms, Analysis, and Applications* (Springer, New York, 2008).

[24] K. Stannigel, M. König, J. Niegemann, and K. Busch, Opt. Express **17**, 14934 (2009).

[25] A. Akhiezer, *Plasma Electrodynamics: Nonlinear Theory and Fluctuations* (Pergamon, New York, 1975), Vol. 2.

[26] Y. Zeng, W. Hoyer, J. Liu, S. W. Koch, and J. V. Moloney, Phys. Rev. B **79**, 235109 (2009).

[27] See Supplemental Material at http://link.aps.org/supplemental/10.1103/PhysRevLett.109.015502 for further results on the theoretical modeling.